Broadly tunable ultrafast pump-probe system operating at multi-kHz repetition rate

Alexander Grupp, Arne Budweg, Marco P Fischer, Jonas Allerbeck, Giancarlo Soavi[1], Alfred Leitenstorfer and Daniele Brida[2]

Department of Physics and Center for Applied Photonics, University of Konstanz, D-78457 Konstanz, Germany

E-mail: daniele.brida@uni-konstanz.de

Abstract

Femtosecond systems based on ytterbium as active medium are ideal for driving ultrafast optical parametric amplifiers in a broad frequency range. The excellent stability of the source and the repetition rate tunable to up to hundreds of kHz allow for the implementation of an advanced two-color pump probe setup with the capability to achieve excellent signal-to-noise performances with sub-10 fs temporal resolution.

Keywords: ultrafast optics, ultrafast spectroscopy, nonlinear optics, optical parametric amplifiers

1. Introduction

Nonlinear optical spectroscopy is an experimental concept that is the cornerstone for the investigation of fundamental light–matter interactions and pump-probe is its workhorse implementation [1–5]. This technique allows for time-resolved experiments in which an ultrashort laser pulse excites impulsively a physical system. After a controlled delay time, a second light pulse probes the transient changes that occurred in the sample. Variations in the intensity of the light transmitted/reflected by the sample are due to induced changes in absorption or refractive index and deliver insights into the evolution of the energetic landscape within the system under study. In fact, information about relaxation dynamics and energy transfer can be acquired by a precise choice of the photon energies exploited for exciting and probing the sample [1–4]. In particular, with two-color pump-probe experiments it is possible to study a wide range of fundamental processes like electron–electron and electron–phonon interactions in solid state systems characterized by broad bands for the description of the electronic states [5–7].

In general, ultrafast relaxation processes can occur on a timescale that can be as short as a few femtoseconds. Therefore, ultrashort laser pulses guarantee the exceptional temporal resolution that is needed for the investigation of the fastest phenomena that follow impulsive excitation. Convenient strategies for the generation of pulses with durations of only a few optical cycles rely on nonlinear optical processes driven by mode-locked and amplified laser systems. Well established ultrafast spectroscopy setups rely on Ti:sapphire technology. These lasers, due to their broadband gain spectrum, deliver pulses with durations below 6 fs directly from the oscillator [8, 9] and of 30 fs at the output of amplification stages. In the last few decades, optical parametric amplifiers (OPAs) driven by ultrafast Ti:sapphire lasers have been developed extensively to provide tunability beyond the fundamental wavelength [5, 10–17]. With this approach, central frequencies from the deep ultraviolet [18] to the mid (MIR) and far infrared (FIR) are possible [15, 19–23]. At the same time, the generation of broadband spectra allows compressed pulses of durations well below 10 fs [10, 24–27]. Recently, new laser amplifier systems based on ytterbium doped host materials have emerged. With an emission wavelength of 1030 nm those lasers can be pumped directly via laser diodes, whereas conventional Ti:sapphire amplifiers require more cumbersome pumping sources. This advantage allows manufacturers to build efficient ultrafast laser systems with small footprints, excellent stability and repetition rates in

---

[1] Current address: Cambridge Graphene Centre, University of Cambridge, Cambridge CB3 0FA, United Kingdom.

[2] This article belongs to the special issue: Emerging Leaders, which features invited work from the best early-career researchers working within the scope of the *Journal of Optics*. Dr Daniele Brida was selected by the Editorial Board of the *Journal of Optics* as an Emerging Leader.

the multi-kHz range. Adaption of the well-known OPA schemes to the Yb^{3+} emission is extremely promising for the generation of ultrashort pulses in a wide spectral range [26, 28–30]. Here, we present an experimental setup that is driven by a regeneratively amplified Yb laser and consists of synchronized OPAs producing few-fs pulses with central wavelengths spanning from the visible (VIS) to the FIR. Stable OPA operation at high repetition rate and well-designed detection schemes enable us to perform low noise measurements for which we employ single channel detection as well as multi-channel detection based on a fast Si line camera resolving the full kHz pulse train.

2. Experimental setup

In order to overcome the gain bandwidth limitation of ytterbium-doped gain media, which have a typical spectral width of approximately 30 nm [31], the combination of an Yb laser with nonlinear conversion stages for the generation of ultrashort pulses is highly beneficial [26, 28, 29]. With this approach it is possible to combine the intrinsic stability of the driving source with the versatility of ultrafast OPAs. Additionally, modern Yb-based amplifier systems allow repetition rates up to hundreds of kHz with pulse energies large enough to pump several OPAs in parallel while Ti:sapphire setups are often limited to repetition rates around 1 kHz or require complex cooling strategies when the average power approaches the 10 W level. The main reason is the simpler scalability of Yb systems owing to the lower quantum defect of the gain medium and the longer lifetime of the lasing transition [32]. In addition, the possibility to pump Yb with reliable laser diodes operating in CW guarantees a high level of stability of the output pulse train. In our experimental system, we employ a 10 W ytterbium:KGW laser from Light Conversion Ltd (PHAROS 10W) as driving source. This source has a repetition rate tunable from 1 to 600 kHz. The pulses are 230 fs long and have an energy of 200 μJ below 50 kHz. This value is reduced at higher frequencies while maintaining the average output power of 10 W. We set the typical operation regime to 50 kHz repetition rate where the pulse energy is sufficient to comfortably pump several nonlinear frequency conversion stages in parallel. At the same time, the high counting statistics can effectively reduce the noise in comparison with 1 kHz systems.

The output power is split equally into four branches with 50 μJ energy each for the operation of several synchronous OPA units as sketched in figure 1. Three noncollinear OPAs (NOPAs) provide wavelengths between 450 nm and 2.1 μm while the fourth is used for the generation of mid-infrared radiation up to 30 μm via difference frequency generation (DFG). We additionally obtain short probe pulses from a compressed white light supercontinuum (WL) generated in YAG or sapphire plates. The detailed description of the parametric stages is reported in the following section.

The output of independent OPAs can be freely combined for two-color pump-probe experiments. One beam is selected for excitation and is referred to as pump. The induced changes in the optical properties of the physical system under study are then
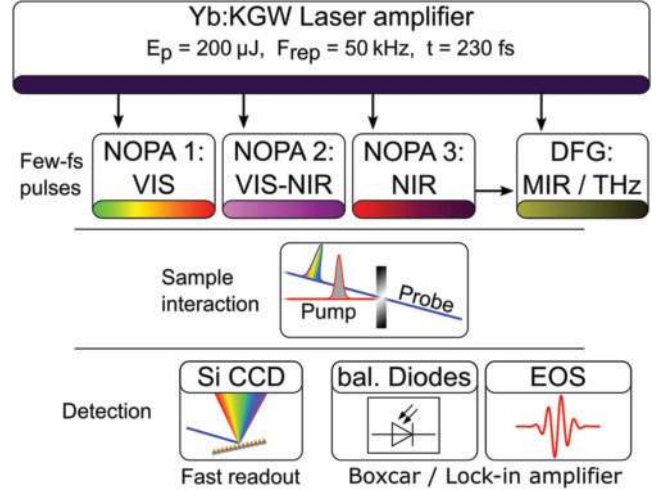

Figure 1. Schematic diagram of the experimental setup. The laser amplifier pumps three parallel OPAs and the DFG stage which can be freely combined for two-color pump-probe experiments. Detection of the probe beam is carried out at 50 kHz with a fast silicon-based CCD spectrometer or with balanced photodiodes. Mid-infrared (MIR) and far-infrared (FIR) pulses are detected via electro electro-optical sampling (EOS).

probed with a second beam. This probe beam is spatially overlapped with the first one on the sample and follows at a time delay τ that can be controlled with sub-fs precision in a correlator equipped with a motorized translation stage. The signal arises from pump induced changes in transmission or reflection of the sample. By precise selection of excitation and detection wavelengths, we match the requirements to study numerous physical systems. Importantly, at low frequencies, mechanical choppers are a convenient method to modulate the pulse train for the detection of differential signals. At higher frequencies, the mechanical modulation introduces detrimental air turbulences and is not optimal. To solve these issues, we developed a new strategy based on non-mechanical pulse modulation employing a Pockels cell (PC). This method facilitates pulse modulation with high optical contrast at frequencies up to 50 kHz.

In addition, we implemented different schemes for the detection of the probe pulses with the goal of minimizing the noise contribution to the experiments in which pump-probe signals can be limited to relative transmission changes of less than 10^{-5}. Balanced photo diodes with a boxcar or lock-in amplifier provide a highly sensitive single channel detection scheme. With common Si or InGaAs photo diodes we cover the spectral range from 300 nm to 2.2 μm. Alternatively, pump-probe signatures might display complex spectral features over broad frequency range. We address this experimental condition by means of a fast spectrometer. This multichannel detector is triggered by the laser system allowing us to read out one full probe spectrum every 20 μs and exploit the high correlation of subsequent laser shots to reach excellent signal-to-noise ratios. Finally, probing in the MIR/FIR spectral region can be performed by detecting the optical transients by electro-optic sampling (EOS). This time-domain scanning technique gives simultaneous access to the amplitude and phase information of the electric field of the probe pulse [33].
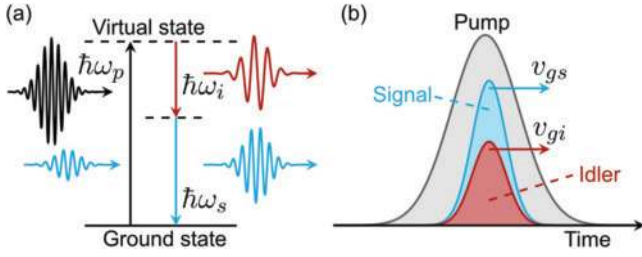
Figure 2. (a) Diagram of the energy conservation in a OPA process, involving pump (p), signal (s) and idler (i) photons. (b) Representation of group velocity matching in a OPA.

The following sections describe in detail the nonlinear conversion stages introduced by our ultrafast setup and all the strategies developed in order to achieve the maxium sensitivity in the detection of transient signals in pump-probe experiments.

3. Broadband sources

Ultrabroadband OPAs are the workhorse tools used for achieving a temporal resolution of less than 10 fs in optical pump-probe experiments. They offer enormous tunability and wide spectra which can be compressed to pulse durations as short as a few optical cycles [10, 34].

The basic concept common to typical OPAs is to provide a weak, but broadband signal beam, which is amplified in a nonlinear crystal exploiting an intense pump beam. This process is described with a second order nonlinear polarization that occurs in non-centrosymmetric crystals, which lacks inversion symmetry, and therefore exhibits a nonlinear $\chi^{(2)}$ susceptibility. Figure 2(a) sketches the energy conservation in a parametric amplification process: a high-energy pump beam ($\hbar\omega_p$) excites a virtual level that is depleted by the spontaneous or stimulated emission of a signal photon ($\hbar\omega_s$), energy conservation requires also the emission of a second photon defined as idler ($\hbar\omega_i$). To obtain significant amplification, signal photons generated at different crystal positions need to interfere constructively. This condition requires matching of the wave vectors (phase velocities) in order to achieve momentum conservation. In common implementations, this phase matching is achieved by exploiting the birefringence of the nonlinear crystal. To achieve broadband amplification the group velocities between signal and idler have to be matched as well. This condition is met in some particular amplification conditions that exploit the refractive index dispersion of the nonlinear crystal or by introducing a non-collinearity angle between pump and signal beams [35, 36]. In this second configuration, the group velocity of the signal (v_{gs}) matches the projection of the idler velocity (v_{gi}) in its own propagation direction as sketched in figure 2(b).

As shown in figure 3, our home-built OPAs provide spectra ranging from 450 nm to 2.1 μm with almost continuous coverage. Depending on the emission wavelength we employ either the fundamental frequency (FF), second harmonic (SH), or the third harmonic (TH) of the Yb laser to pump the nonlinear frequency conversion. The NOPAs in the near infrared (NIR) and visible to near-infrared spectral range (VIS-NIR) are pumped by the SH. Generation of pulses in the VIS requires pumping with the TH. Only MIR and FIR generation are carried out directly with the FF. Additionally we use up to 2 μJ of the FF to generate a white light supercontinuum. Those WL pulses are used for seeding of the NOPAs as well as an alternative pulse source for probing. All these parallel stages are optimized in order to deliver the shortest pulses possible at the best conditions of pulse-to-pulse stability and beam quality.

3.1. Supercontinuum pulses

Broadband spectra can be conveniently generated by exploiting the so-called white light generation that occurs when an intense pulse propagates in a dielectric medium. Third-order nonlinearity (self-phase modulation) and filamentation [37, 38] lead to spectral broadening. These pulses can be effectively used as a probe in ultrafast experiments or alternatively they can be amplified in OPA stages for the generation of intense pump beams.

In contrast to supercontinua obtained from photonic crystal fibers, where often significant spectral modulations occur, solid state bulk materials offer smooth and extremely broadband spectra. When driving pulse energies at the μJ level are used, spectra well suited for the use in OPAs can be generated from crystals such as sapphire [39–41]. Due to the large band gap in this material it is possible to generate wavelengths approaching the UV. Additionally, damage thresholds are found to be very high which allows continuous operation without optical damage. Similar properties are also found in YAG crystals [42]. Compared to sapphire, continua from YAG crystals result in being more stable at higher repetition rates and at longer pumping wavelengths like 1030 nm. All OPAs are seeded with a white light generated in a YAG crystal. The experimental setup for continuum generation is rather simple. A portion of the fundamental beam starting from a diameter of 2.5 mm full width at half maximum (FWHM) is shaped by an iris aperture and focused with a focal length of 100 mm into the crystal. A variable attenuator (VA) allows precise adjustment of the peak intensity at the focal spot. We obtain stable white light emission starting from 90 GW cm^{-2}. Figure 4 displays two white light spectra optimized for the generation of VIS and NIR spectral components, respectively. In detail, with a peak intensity of 180 GW cm^{-2}, we generate a continuum in the visible spectral range covering wavelengths from 450 nm to 1 μm (left, blue area). Even higher peak intensities of 360 GW cm^{-2} allow pushing the short wavelength cut-off to 400 nm (dashed black line) at the cost of spectral intensity around 700 nm. At intermediate peak intensities of 250 GW cm^{-2}, we obtain good conditions for a supercontinuum at IR wavelengths (figure 4 right, yellow area).

Beside its purpose to seed OPAs, we also use selected spectral windows of the white light as a probe in our experiments. By separating the VIS components, we obtain a spectrum which supports a Fourier-transform-limited duration
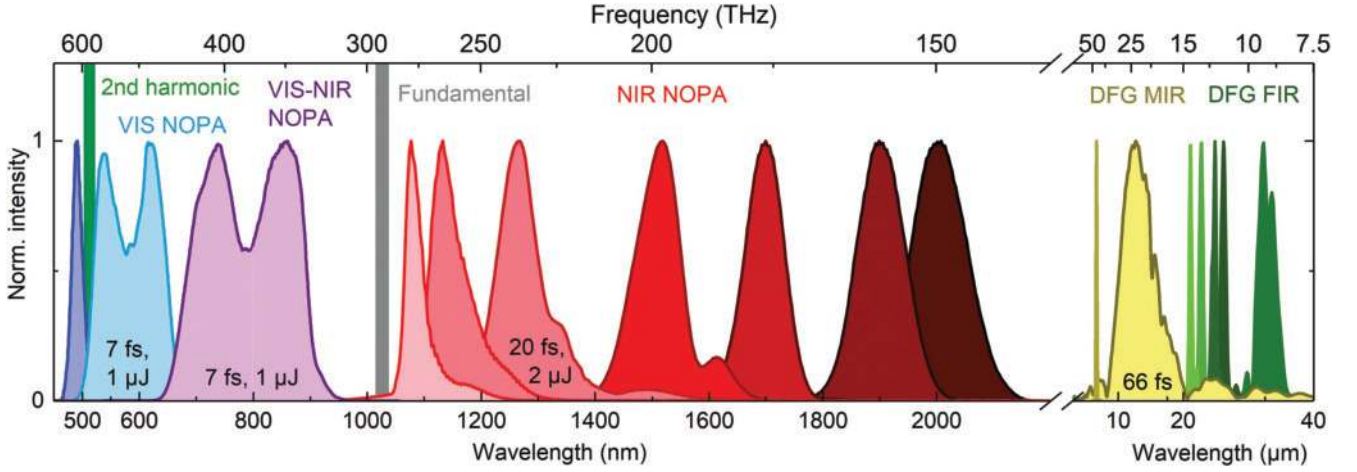
Figure 3. Intensity spectra of our home built OPAs. The combination of VIS, VIS-NIR and NIR NOPAs yields almost gapless spectral coverage from 450 to 2100 nm. MIR and FIR pulses are obtained from DFG in GaSe and 4H-SiC of the first harmonic with the NIR NOPA. Pulse durations and pulse energies of selected configurations are displayed.
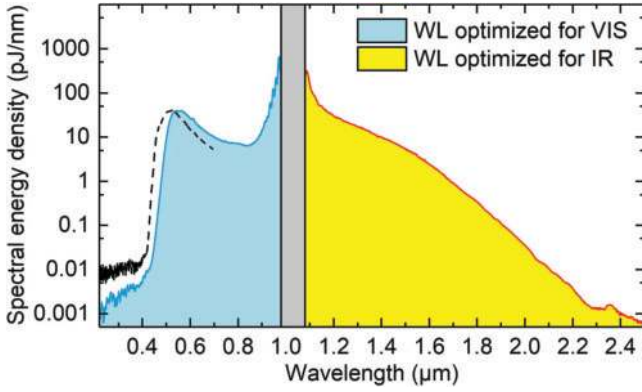

Figure 4. Spectral energy density of the white light supercontinuum generated in a 4 mm YAG crystal. Pump pulse energy and focusing was optimized individually for optimum conditions at wavelengths shorter (left, blue area) and longer (right, yellow area) than the fundamental wavelength. At high intensities the short wavelength cut off shifts at cost of intermediate wavelengths (dashed black). The gray area is blocked with color filters and includes the pump wavelength of 1030 nm.

Figure 5. Schematic of the VIS-NIR NOPA. After non-collinear superposition of pump (green) and signal beam (blue) we use a pair of dielectric chirped mirrors (DCM) or alternatively a prism compressor (dashed box) for pulse compression.

of only 3 fs. Even without any pulse compression a few-fs time resolution is possible by spectral filtering of the probe pulses prior to detection [43]. Nevertheless, compression of the probe pulses yields advantages. A pair of dielectric chirped mirrors serves for pulse compression in the spectral range from 450 to 750 nm, where a pulse duration of approximately 7 fs is obtained. As a result, the retrieved constant spectral phase allows the evaluation of broadband spectral signatures without any further correction of the time delay in pump-probe experiments. Also, the infrared portion of our white light is of interest for being employed as probe beam in time-resolved experiments. Here, dispersion compensation is provided by means of an SF10 prism pair with 61° apex angle and a distance of 140 mm. Short wavelength components around 1050 nm close to the fundamental exhibit a steeper phase as compared to longer wavelengths. For that reason, we select the spectrum with a razor blade placed in the Fourier plane of the prism compressor. Pulse characterization
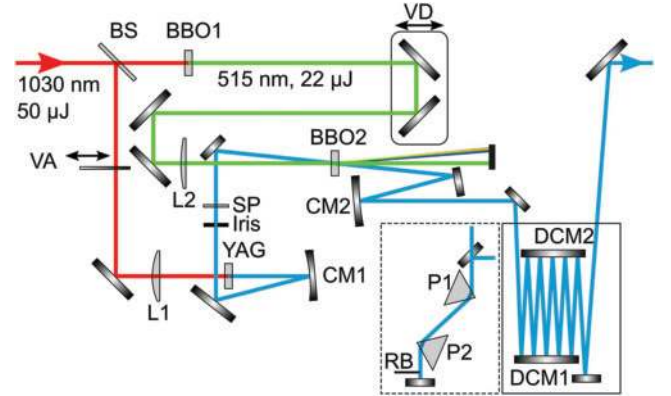
is carried out via second-harmonic-generation frequency-resolved optical gating (FROG) [44] and yields pulse durations of 14 fs whereas the full IR spectrum shown in figure 4 possesses a transform limited duration of 9.5 fs. Beside pump-probe experiments, these pulses are well suited to be employed as gates in electro optical sampling. We use them for field resolved detection of THz pulses with frequency components up to 50 THz.

3.2. Generation of pulses in the visible to NIR

The basic layout of the NOPA follows the traditional schemes as used with Ti:sapphire systems [10, 24, 26, 34]. Figure 5 presents a schematic representation of the VIS-NIR NOPA. We split a small portion from the 50 μJ fundamental beam for supercontinuum generation in a 2 mm thick YAG crystal. With a VA we tune the pulse energy to achieve optimum conditions. The white light is collimated by a curved mirror (CM1) and spectrally filtered with a short pass filter (SP) at 900 nm to avoid amplification of spurious wavelengths. It should be remarked that the filamentation process produces
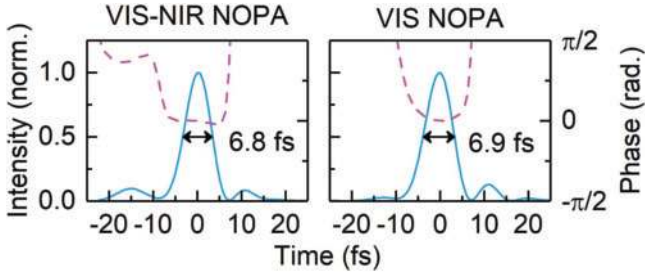
Figure 6. Reconstructed temporal profile (blue, solid) and phase (pink, dashed) from SHG- FROG traces of the VIS-NIR NOPA and VIS NOPA.
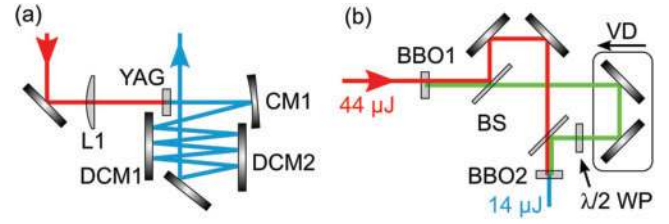

Figure 7. (a) Temporal compression of white light pulses with dielectric chirped mirrors (DCM) prior to the parametric amplification stage allows for the generation of extremely broadband VIS pulses. (b) Third harmonic generation with 32% efficiency via two separate conversion steps. Frequency doubling (BBO1) is followed by sum-frequency generation (BBO2).

spectra that are not well-behaved in the proximity of the driving wavelength.

The main portion of the pump light is frequency doubled in a BBO crystal. For this task, we exploit type-I phase-matching ($\theta = 24°$) in a 2 mm thick crystal. After rejecting the residual fundamental wavelength with dielectric mirrors, we obtain 22.5 μJ pulse energy at 515 nm with a 50% conversion efficiency for pumping the OPA. A variable delay line adjusts the timing between the pulses. The pump beam is then focused with a focal length of 200 mm. We set the focal plane several centimetres before the nonlinear medium yielding a peak intensity of 130 GW cm^{-2} inside the 1.5 mm thick BBO crystal, which is used for the mixing process. Broadband amplification is achieved at the phase matching angle of $\theta = 24°$ when pump and signal beams form an internal angle of $\alpha = 2.6°$. The amplified signal is collimated by a second curved mirror (CM2). Finally, we use dielectric chirped mirrors (DCM1 and DCM2) for dispersion compensation. The resulting spectrum is shown in figure 3 as VIS-NIR NOPA. We characterize the temporal profile of our pulses by means of SHG FROG and obtain a duration of below 7 fs as depicted in the reconstructed intensity profile (figure 6). The transform-limited duration is 5.6 fs.

3.3. Generation of pulses in the NIR

With slight modifications of the experimental layout presented in figure 5 we can adapt the NOPA spectrum to the NIR spectral region. Optimum conditions for white light generation at 1.2 μm are found when using a 5 mm thick YAG crystal. Spectral selection with a long pass filter at 1064 nm allows us to exploit a broad frequency range generated by the WL process.

The pump branch is frequency doubled as described above but we reduce the peak intensity inside the parametric conversion BBO to 50 GW cm^{-2} by extending the focal length to 300 mm. The NOPA still operates with 10% signal-to-pump efficiency in this condition and exhibits improved long-term stability. Broadband amplification occurs at the phase matching angle of $\theta = 23.1°$ when pump and signal beams form an internal angle of $\alpha = 2.6°$. By slight tuning of phase matching and non-collinearity angles we access spectral components from 1070 nm to 2.1 μm as shown in figure 3 as NIR NOPA. For pulse compression, we use SF56 glass Brewster prisms, cut at an angle of $59.4°$ with an apex

distance of 220 mm. A SHG FROG characterization yields 20 fs pulse duration at 1300 nm central wavelength.

3.4. Generation of pulses in the visible

Accessing spectral components in the VIS range adds slightly more complexity to the setup of the NOPA [26]. For the seed generation, we focus the fundamental wavelength with a focal length of 100 mm into a 3 mm thick YAG crystal. The resulting supercontinuum extends to wavelengths as short as 450 nm but is strongly chirped. Prior to amplification, we therefore precompress the white light with specially designed dielectric chirped mirrors (figure 7(a)).

This NOPA is pumped by the TH of the fundamental wavelength. Figure 7(b) depicts the pump conversion setup. In a first BBO crystal, we generate the SH similar to what discussed previously. We then separate the FF and SH components by means of a dichroic beam splitter, rotate the polarization of the SH by $90°$ and overlap both beams in a second BBO crystal of 2 mm thickness cut for type-I phase matching ($\theta = 32.5°$). In this branch, we achieve 14 μJ pulse energy at 343 nm wavelength with an upconversion efficiency of 32%. For the parametric amplification stage, the pump beam is focused with an $f = 200$ mm lens and the BBO crystal is placed 30 mm behind the focal plane. The pump-signal angle is adjusted to $4.5°$ where we obtain broadband amplification with type-I phase matching ($\theta = 37°$). The resulting spectrum is depicted in figure 3 as VIS NOPA. By means of a second pair of chirped mirrors, we compress the NOPA pulses. Figure 6 depicts the reconstructed intensity profile where a pulse duration below 7 fs is obtained while a Fourier-limited duration of 5 fs is supported by the spectrum.

3.5. Generation of pulses in the MIR

One intuitive way to generate MIR wavelengths is to exploit the idler wave of an OPA [12, 45]. A second route employs DFG from two NIR pulses [20, 46]. Both approaches can rely on crystals like gallium-(II)-selenide (GaSe) since it offers a large transmission bandwidth in the MIR, a high second-order nonlinear coefficient and the possibility for birefringent phase matching which render it perfect for MIR frequency mixing [47].
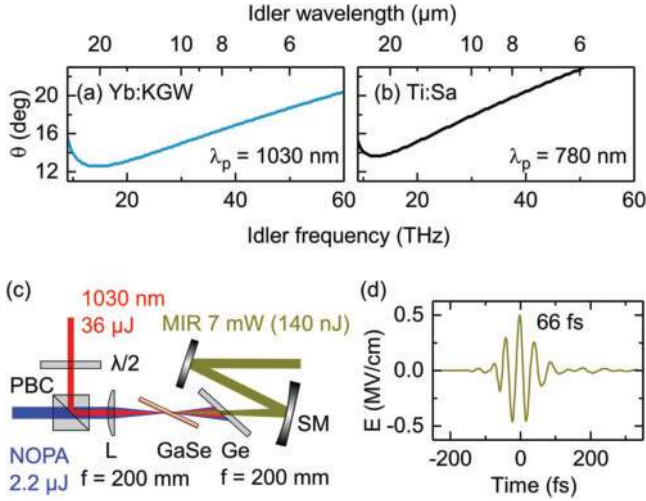
Figure 8. (a) Phase matching angle θ for DFG of the FF with the NIR NOPA in a gallium-selenide crystal (GaSe). (b) Tuning range when the fundamental frequency of Ti:sapphire is used. (c) Scheme for generation of MIR pulses via DFG. Residual NIR components are filtered with a germanium wafer (Ge). (d) Electric field of the MIR pulses reconstructed by electro-optical sampling. Peak fields of $0.5 \, \mathrm{MV \, cm^{-1}}$ are obtained when focusing the pulses with an all reflective objective to a spot size of 20 μm.

To obtain a high conversion efficiency, we implement the approach of DFG inspired by multi-THz generation driven with Ti:sapphire systems [48]. In detail, we can drive the DFG process between the fundamental wavelength of our laser system at 1030 nm and the spectrum generated from the tunable NIR NOPA. With this scheme we can generate MIR wavelengths spanning from 7.5 to 30 μm (10 to 20 THz). Calculations for type-II phase matching (figure 8(a)) display the tuning range of the DFG driven at 1030 nm compared to pumping with the Ti:sapphire wavelength at 780 nm (b). Remarkably, the red-shifted FF of the Yb laser allows for a broader phase matching condition as highlighted by the shallow dispersion of the phase matching angle in particular between 10 and 20 THz. In light of this favorable condition, a scheme requiring DFG between two NIR OPAs is not a significant improvement and would be intrinsically less efficient.

Within our experimental implementation, we overlap the FF (36 μJ at 1030 nm) and the output of the NIR NOPA (2.2 μJ) tuned at approximately 1200 nm with a polarizing beam splitter to be perfectly collinear. We focus the beams with an $f = 200$ mm lens, whereas the nonlinear crystal is placed 55 mm behind the focal plane. For the generated pulses, GaSe crystals of thicknesses between 100 μm and 1 mm allow to trade-off large bandwidth with shorter crystals against intensity in longer ones. Figure 3 reports the spectra (solid green) that can be obtained by tuning the OPAs central wavelength and thus the DFG frequency. With EOS, we reconstruct the electric field of the multi-THz pulses. As a gating pulse, we employ the infrared components of our white light supercontinuum. After pulse compression, durations of 14 fs are achieved, which allows to sample frequencies up to 50 THz. Figure 8(d) depicts a typical Fourier-limited pulse

with a duration of 66 fs FWHM and peak electric fields of $0.5 \, \mathrm{MV \, cm^{-1}}$ in the focal plane when focusing to a spot size of 20 μm. Spectral regions below 15 THz, where phonon resonances in most crystals hinder frequency mixing, can be reached by using silicon carbide (4H-SiC) [49] as nonlinear emitter.

4. Pump-probe system

The transient absorption/reflection experiments are carried out in a two color interferometer. We evaluate differential changes in the intensity of the probe pulses transmitted (or reflected) by the pumped and un-pumped sample: $\frac{I_{pumped} - I_{unpumped}}{I_{unpumped}} = \frac{\Delta I}{I}$. Such a signal is then measured as a function of the delay between the two pulses. The differential changes usually amount to less than one percent of the probe pulse intensity. Thus, a detection scheme based on a modulation technique is needed in order to resolve the small signals. A common realization periodically blocks the pump pulses and by this imprints the signal onto the probe pulse train at the frequency of the pump modulation.

Pulse-to-pulse correlations are high when comparing subsequent transients of a pulse train and decrease when pulses are separated by multiple periods of the repetition rate. We therefore introduce a scheme for fast modulation at half of the repetition rate based on a PC. With this modulation, we evaluate subsequent laser shots of the probe $(I_{j+1}-I_j)/I_j$ and average the differential signal.

The concept for this modulation is to rotate the polarization plane of every second pulse and separate them with a polarization-dependent beam splitter. However, due to the dispersion of the nonlinear crystals an efficient half-wave operation is not possible with broadband spectra as the ones generated in the NOPAs. Placing the PC in the fundamental beam before the NOPA leads to nonlinear effects, such as self-phase modulation and self-focusing in the cm-long electro-optic crystal due to the high pulse energies and can ultimately lead to optical damage. We circumvent this problem by positioning the PC directly in front of the white light generation as shown in figure 9(a). There the pulse energies are moderate and the narrowband spectrum allows proper half-wave operation. The cell contains two potassium titanyl phosphate (KTP) crystals with 10 mm thickness each and is operated with a half-wave voltage of 2.4 kV. We generate the high-voltage signal from a trigger that is directly locked to the laser repetition rate. Any phase slips or beating is intrinsically avoided. Influences of the KTP dispersion on the fundamental beam are negligible since pulse broadening in the crystal amounts to less than 1% of the initial temporal duration of 230 fs. The red graph in figure 9(c) shows the modulated pulse train detected by a photo diode. We obtain an intensity contrast of 1:50. Due to the highly nonlinear behavior of the supercontinuum generation, this ratio is enough to switch off the white light generation process completely. A measurement of the pulse intensity at the sample position, depicted in the right panel of figure 9(c), shows evidence that also the
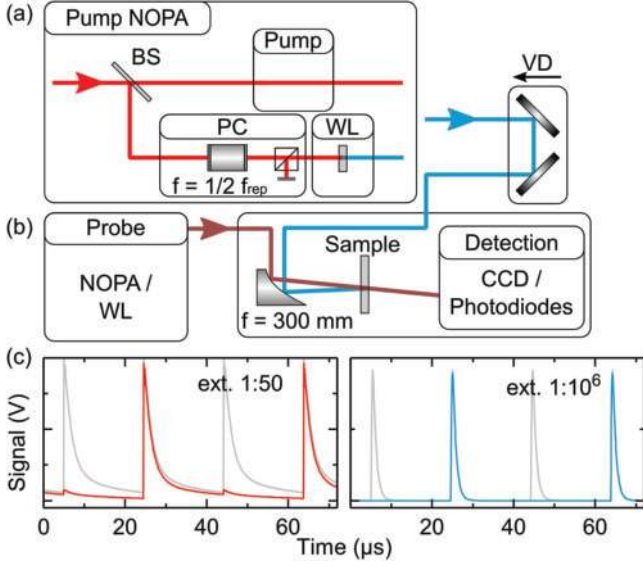
Figure 9. Schematic showing a NOPA with a Pockels cell (PC) for fast modulation at $f_{rep}/2$ of the seed beam operating as pump branch (a) and a NOPA/white light probe (b) used for transient absorption experiments. (c) Oscilloscope measurements of the modulated pulse train before the white light generation (left, red) and at the sample position (blue, right) with an extinction factor exceeding 10^6.

parametric superfluorescence in the unseeded NOPA is negligible. We obtain a contrast better than $1:10^6$ limited only by the resolution of the oscilloscope used for this characterization. Compared to conventional modulation techniques such as mechanical choppers, we achieve modulation frequencies up to the repetition rate of our laser (50 kHz) and avoid any moving components in the beam path that could lead to additional noise.

When planning an experiment, we place the PC in the NOPA used for excitation. Probe pulses can be supplied from a second NOPA or the compressed white light source. Both pulses are coupled into the two branches of the correlator. With curved mirrors, we reduce the spot size to approximately 100 μm and overlap both beams at the sample position. By using all reflective optics, we maintain the ultrashort pulse durations. A small angle between pump and probe allows convenient spatial filtering of the pump pulses after the sample without affecting the temporal resolution.

4.1. Noise performance and single-channel detection

In order to be able to detect small signals, we carefully minimized the noise contributions in the generation of the NOPA pulses and in the detection used in pump-probe experiments. For white light generation precise adjustment of the laser intensity and mode shape are crucial to obtain stable emission. In optimal conditions, the WL displays rms fluctuations of 0.12%, measured over 20 min with a detection bandwidth of 50 kHz, i.e. recording every single laser shot with a boxcar integrator. Figure 10(a) shows the relative energy of each laser pulse in the white light measured after spectral filtering at 550 nm with an optical bandwidth of 14 nm. This characterization demonstrates that the WL is also
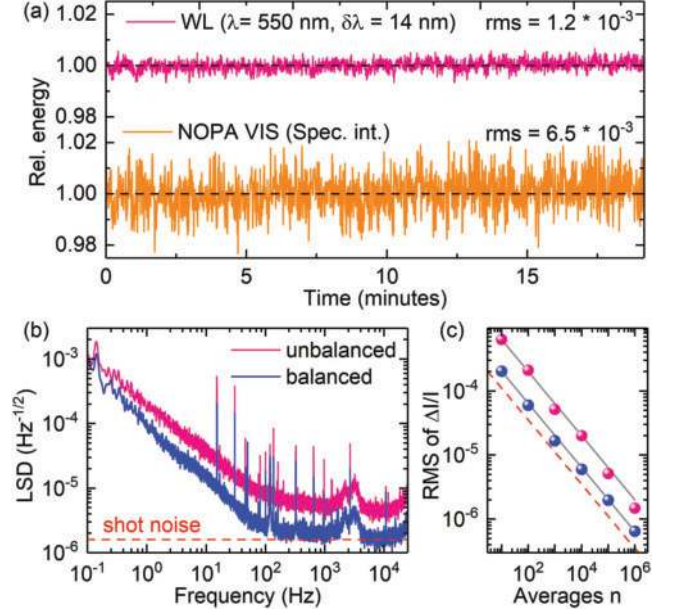

Figure 10. (a) Relative pulse energy as a function of time for the white light (WL) and the VIS NOPA. (b) Linear spectral density (LSD) normalized to the average power for the white light probe in single beam (unbalanced) and balanced (balanced) configuration. (c) Rms of the differential signal $\Delta I/I$ as a function of averages for both probe configurations. Solid lines represent $1/\sqrt{n}$ fits indicating good statistical averaging possibilities. The shot noise level is marked as dashed line.

spectrally stable. Results obtained with the multi-channel detection confirm the wavelength independent noise level. The lower graph in figure 10(a) depicts the spectrally integrated measurement of the VIS NOPA where we observe a slightly higher average noise value of 0.65% rms fluctuations. Both graphs show an excellent long term stability, which enables us to perform data acquisition and averaging over several hours.

To improve signal-to-noise even further, we employ a balanced detection scheme that suppresses the laser fluctuations down to the shot noise limit. Therefore, a portion of the probe beam is split off prior to interaction with the sample. We pass this reference beam at a temporal offset through the sample and through the same monochromator as the probe beam. Afterwards we detect both probe replicas with a balanced circuit in which two diodes are wired for subtracting their photocurrents. Technical noise contributions originating from the laser system cancel whereas the pump-probe signal remains. With the reference beam included, the noise floor of our white light probe drops to 3.7×10^{-4} rms in the relative amplitude of the pulses. The average energy of 45 pJ yields a shot noise level of 3.6×10^{-4} rms. Figure 10(b) depicts the linear spectral density (LSD) normalized to the average power of the probe beam. We observe an improvement due to the balanced detection over the entire spectral range. At frequencies above 500 Hz, our detection becomes limited by the shot noise of the photo current. A narrow band detection like a lock-in amplifier is therefore best used with high modulation frequencies which can be realized with the PC modulation scheme. Figure 10(c) displays the differential signal ($\Delta I/I$) of
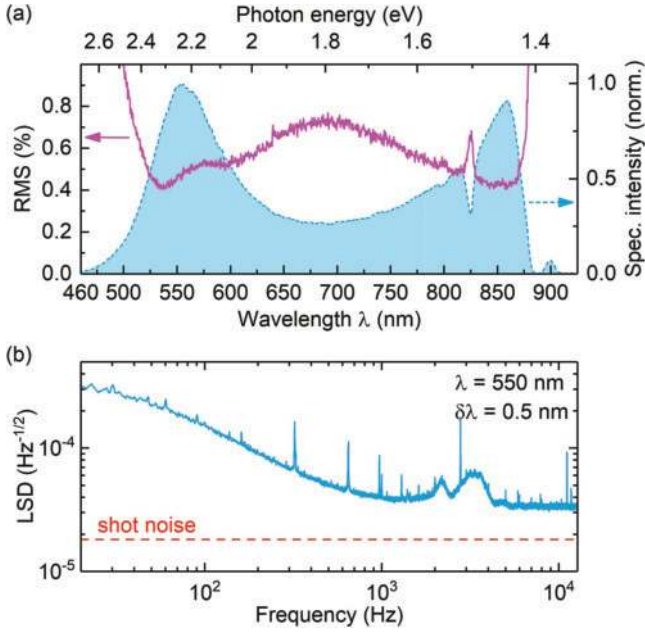
Figure 11. (a) Intensity spectrum of the white light probe recorded with the fast spectrometer (dashed blue) and rms fluctuations at each pixel (pink). (b) Linear spectral density normalized to the average power for the white light probe detected with the fast spectrometer.

an experimental pump-probe run with 10^6 averages. With and without the balanced detection, the differential signal decreases with the root of evaluated averages indicated by the $1/\sqrt{n}$ fits displayed as gray lines. We are able to reach a noise level of 6.5×10^{-7} with our white light probe.

4.2. Multi-channel detection

For studies which involve rich spectral signatures, it becomes time consuming to sample broadband probe spectra with a monochromator. Enormous improvement is achieved with a multi-channel detection. For this purpose, we employ a specially developed spectrometer (Entwicklungsbüro G. Stresing, Germany) which consists of a polychromator (Acton SP-2156) in combination with a fast silicon CCD detector (Hamamatsu S11490). The detector is triggered by the laser system and it is possible to read out spectra with a rate of up to 50 kHz at a maximum modulation rate of 25 kHz. This fast acquisition works hand in hand with the pump beam modulation achieved by the PC. It allows us to subtract consecutive spectra to retrieve a wavelength dependent pump-probe signal. Figure 11(a) shows the normalized intensity spectrum of the WL probe as detected by the camera. Its pulse energy ensures sufficient illumination of our sensor so that the supercontinuum can be efficiently used for probing. This approach is slightly advantageous compared to a NOPA pulse probe as the latter exhibits slightly higher fluctuations and lower long term stability. With optimum illumination of our sensor, we observe rms fluctuations of 0.4% on a single pixel. One pixel corresponds to an optical bandwidth of 0.5 nm and this detection schemes approach exceeds the shot noise limit by less than a factor of two. The noise level at different detection wavelengths corresponds to the intensity at the
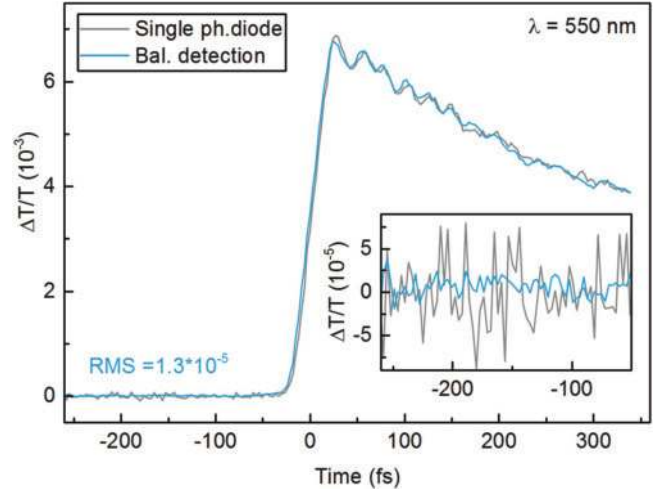

Figure 12. $\Delta T/T$ signal as function of time delay after averaging 1000 pump-on pump-off pairs of the white light probe. The noise level decreases to 1.3×10^{-5} by including the reference beam for the balanced detection. The whole scan is performed in approximately 10 s in both configurations.

individual pixels and is therefore dominated by the technical noise of the CCD. Spectral fluctuations in the supercontinuum are negligible. In situations where spectral resolution is not required to be in the sub-nm range, averaging over adjacent pixels reduces the noise level. The LSD plot in figure 11(b) is again normalized to the average power and is acquired at the pixel corresponding to 550 nm of our probe spectrum. The noise floor is minimal at modulation frequencies higher than several kHz. In this situation, it is again favorable to perform the evaluation of the differential pump-probe signal at the high modulation rate provided by the PC.

4.3. Ultrafast spectroscopy

In this subsection, we demonstrate the use of the experimental apparatus described above for tracking ultrafast phenomena in condensed matter systems. The model sample is a 30 nm thick layer of poly(3-hexylthiophene) (P3HT) spin-coated on a thin fused silica substrate. This conjugated polymer is often used for opto-electronic applications like organic photovoltaics [50] and has been extensively studied in ultrafast experiments. In detail, P3HT possesses a broadband optical absorption in the visible spectral range which can be excited impulsively by pulses from the short VIS NOPA. The following dynamical evolution of the system is characterized by ultrafast relaxation and coherent phonons which allow us to assess the capabilities of the experimental setup.

First, we discuss results obtained with the single channel detection using the monochromator, balanced photodiodes and detection via the boxcar gated integrator. Figure 12 shows the differential transmission change when the polymer is excited with the VIS NOPA centered at 577 nm. We probe with white light pulses generated in a sapphire plate and set the monochromator to 550 nm. The graph displays the differential transmission signal as a function of the pump-probe delay after averaging 1000 consecutive pump-on and pump-off pairs for
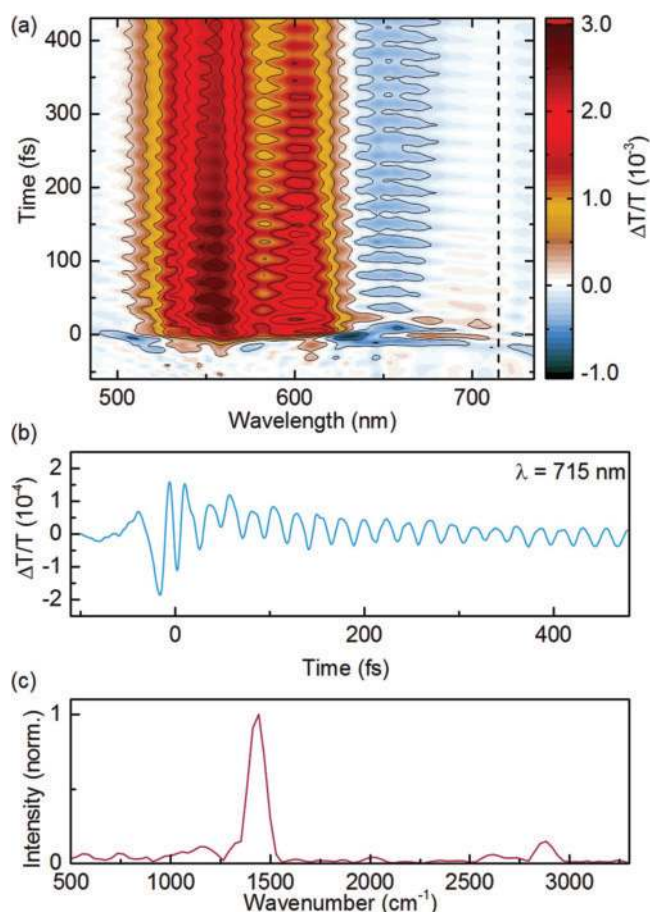
Figure 13. (a) $\Delta T/T$ signal as a function of time delay and probe wavelength. (b) Dynamics at $\lambda = 715$ nm display a fast oscillatory behavior. (c) Fourier transform of (b) as function of wavenumber showing two pronounced peaks at 1450 and 2900 cm^{-1} which can be assigned to vibrational modes of the excited polymer.

from the Fourier transform (figure 13(c)) of the oscillatory pattern that unveil coherent phonons up to frequencies of approximately 2900 cm^{-1} (symmetrical CH_2 stretching mode [51]) assessing a temporal resolution of 10 fs.

5. Conclusion

We presented an advanced spectroscopy system that fully exploits the advantages of Yb laser systems for achieving 10 fs temporal resolution in pump-probe experiments requiring exceptional low noise levels. In particular, we demonstrate that it is possible to design a class of broadband OPAs which generate pulses covering a wavelength range from 450 to 2100 nm and also span the mid and FIR. These sources are intrinsically synchronized allowing for multi-color spectroscopy at high repetition rates. The clear benefits of this system are its versatility and its capability to detect small signals as the ones arising from isolated quantum objects or layered materials. High frequency modulation, noise suppression, broadband nonlinear conversion stages, and sub-10 fs temporal resolution are the fundamental ingredients that will push ultrafast spectroscopy to investigate even more subtle phenomena at the core of light–matter interaction.

ORCID iDs

Daniele Brida https://orcid.org/0000-0003-2060-5480

each temporal data point. A zoom into the signal at negative delay times clearly shows the difference between the single diode and the balanced detection. With balancing, we observe rms fluctuations of 1.3×10^{-5} in contrast to 3.7×10^{-5} with a single diode. At positive delay times, our signal is modulated and exhibits an oscillatory component with a periodicity of 23 fs. We attribute this signal to a coherent C=C stretching vibrational mode of the polymer [51], which can only be excited and detected due to the high overall temporal resolution guaranteed by the ultrashort pulses employed in the experiment.

Furthermore, we use the same P3HT film to demonstrate the capabilities of the probe detection with the fast spectrometer. The sample is excited with the VIS NOPA centered at 577 nm and transmission changes are probed again with a white light supercontinuum. Figure 13(a) shows the retrieved differential transmission as a function of time delay and probe wavelength. Spectra were recorded at 200 different time delays between pump and probe pulse and the total data acquisition took about one hour. At wavelengths longer than 700 nm we observe small pump-probe signatures of 1×10^{-4} whereas the noise floor is kept below 10^{-5} (see figure 13(b)). Even with such low signals, we extract two distinct peaks

References

[1] Knox W H, Hirlimann C, Miller D A B, Shah J, Chemla D S and Shank C V 1986 Femtosecond excitation of nonthermal carrier populations in GaAs quantum wells *Phys. Rev. Lett.* **56** 1191–3

[2] Laubereau A, von der Linde D and Kaiser W 1972 Direct measurement of the vibrational lifetimes of molecules in liquids *Phys. Rev. Lett.* **28** 1162–5

[3] Shank C V, Fork R L, Leheny R F and Shah J 1979 Dynamics of photoexcited GaAs band-edge absorption with subpicosecond resolution *Phys. Rev. Lett.* **42** 112–5

[4] Zewail A H 2000 Femtochemistry: atomic-scale dynamics of the chemical bond *J. Phys. Chem.* A **104** 5660–94

[5] Brida D *et al* 2013 Ultrafast collinear scattering and carrier multiplication in graphene *Nat. Commun.* **4** 1987

[6] Soavi G, Grupp A, Budweg A, Scotognella F, Hefner T, Hertel T, Lanzani G, Leitenstorfer A, Cerullo G and Brida D 2015 Below-gap excitation of semiconducting single-wall carbon nanotubes *Nanoscale* **7** 18337–42

[7] Trushin M *et al* 2015 Ultrafast pseudospin dynamics in graphene *Phys. Rev.* B **92** 165429

[8] Sutter D H, Steinmeyer G, Gallmann L, Matuschek N, Morier-Genoud F, Keller U, Scheuer V, Angelow G and Tschudi T 1999 Semiconductor saturable-absorber mirror–assisted Kerr-lens mode-locked Ti:sapphire laser producing pulses in the two-cycle regime *Opt. Lett.* **24** 631

[9] Morgner U, Kärtner F X, Cho S H, Chen Y, Haus H A, Fujimoto J G, Ippen E P, Scheuer V, Angelow G and Tschudi T 1999 Sub-two-cycle pulses from a Kerr-lens mode-locked Ti:sapphire laser *Opt. Lett.* **24** 411

[10] Baltuska A, Fuji T and Kobayashi T 2002 Visible pulse compression to 4 fs by optical parametric amplification and programmable dispersion control *Opt. Lett.* **27** 306–8

[11] Wilhelm T, Piel J and Riedle E 1997 Sub-20 fs pulses tunable across the visible from a blue-pumped single-pass noncollinear parametric converter *Opt. Lett.* **22** 1494

[12] Brida D, Manzoni C, Cirmi G, Marangoni M, De Silvestri S and Cerullo G 2007 Generation of broadband mid-infrared pulses from an optical parametric amplifier *Opt. Express* **15** 15035

[13] Brida D, Cirmi G, Manzoni C, Bonora S, Villoresi P, De Silvestri S and Cerullo G 2008 Sub-two-cycle light pulses at 1.6 μm from an optical parametric amplifier *Opt. Lett.* **33** 741

[14] Fu Y, Takahashi E J and Midorikawa K 2015 High-energy infrared femtosecond pulses generated by dual-chirped optical parametric amplification *Opt. Lett.* **40** 5082

[15] Yin Y, Ren X, Chew A, Li J, Wang Y, Zhuang F, Wu Y and Chang Z 2017 Generation of octave-spanning mid-infrared pulses from cascaded second-order nonlinear processes in a single crystal *Sci. Rep.* **7** 11097

[16] Yin Y, Li J, Ren X, Zhao K, Wu Y, Cunningham E and Chang Z 2016 High-efficiency optical parametric chirped-pulse amplifier in BiB_3O_6 for generation of 3 mJ, two-cycle, carrier-envelope-phase-stable pulses at 17 μm *Opt. Lett.* **41** 1142

[17] Kessel A, Trushin S A, Karpowicz N, Skrobol C, Klingebiel S, Wandt C and Karsch S 2016 Generation of multi-octave spanning high-energy pulses by cascaded nonlinear processes in BBO *Opt. Express* **24** 5628

[18] Baum P, Lochbrunner S and Riedle E 2004 Tunable sub-10 fs ultraviolet pulses generated by achromatic frequency doubling *Opt. Lett.* **29** 1686–8

[19] Petrov V, Rotermund F, Noack F and Schunemann P 1999 Femtosecond parametric generation in ZnGeP$_2$ *Opt. Lett.* **24** 414–6

[20] Seifert F, Petrov V and Woerner M 1994 Solid-state laser system for the generation of midinfrared femtosecond pulses tunable from 3.3 to 10 microm *Opt. Lett.* **19** 2009–11

[21] Junginger F, Sell A, Schubert O, Mayer B, Brida D, Marangoni M, Cerullo G, Leitenstorfer A and Huber R 2010 Single-cycle multiterahertz transients with peak fields above 10 MV/cm *Opt. Lett.* **35** 2645–7

[22] Yin Y, Chew A, Ren X, Li J, Wang Y, Wu Y and Chang Z 2017 Towards Terawatt Sub-cycle long-wave infrared pulses via chirped optical parametric amplification and indirect pulse shaping *Sci. Rep.* **8** 45794

[23] Sanchez D, Hemmer M, Baudisch M, Cousin S L, Zawilski K, Schunemann P, Chalus O, Simon-Boisson C and Biegert J 2016 7 μm, ultrafast, sub-millijoule-level mid-infrared optical parametric chirped pulse amplifier pumped at 2 μm *Optica* **3** 147

[24] Shirakawa A, Sakane I, Takasaka M and Kobayashi T 1999 Sub-5 fs visible pulse generation by pulse-front-matched noncollinear optical parametric amplification *Appl. Phys. Lett.* **74** 2268–70

[25] Kobayashi T and Baltuska A 2002 Sub-5 fs pulse generation from a noncollinear optical parametric amplifier *Meas. Sci. Technol.* **13** 1671–82

[26] Liebel M, Schnedermann C and Kukura P 2014 Sub-10 fs pulses tunable from 480 to 980 nm from a NOPA pumped by an Yb:KGW source *Opt. Lett.* **39** 4112

[27] Cerullo G, Nisoli M, Stagira S and De Silvestri S 1998 Sub-8 fs pulses from an ultrabroadband optical parametric amplifier in the visible *Opt. Lett.* **23** 1283–5

[28] Steinmann A, Killi A, Palmer G, Binhammer T and Morgner U 2006 Generation of few-cycle pulses directly from a MHz-NOPA *Opt. Express* **14** 10627–30

[29] Homann C, Schriever C, Baum P and Riedle E 2008 Octave wide tunable UV-pumped NOPA: pulses down to 20 fs at 0.5 MHz repetition rate *Opt. Express* **16** 5746–56

[30] Deng Y *et al* 2012 Carrier-envelope-phase-stable, 12 mJ, 15 cycle laser pulses at 21 μm *Opt. Lett.* **37** 4973

[31] Agnesi A, Greborio A, Pirzio F, Reali G, Aus der Au J and Guandalini A 2012 40 fs Yb(3+):CaGdAlO4 laser pumped by a single-mode 350-mW laser diode *Opt. Express* **20** 10077

[32] Fischer J, Heinrich A-C, Maier S, Jungwirth J, Brida D and Leitenstorfer A 2016 615 fs pulses with 17 mJ energy generated by an Yb:thin-disk amplifier at 3 kHz repetition rate *Opt. Lett.* **41** 246

[33] Huber R, Brodschelm A, Tauser F and Leitenstorfer A 2000 Generation and field-resolved detection of femtosecond electromagnetic pulses tunable up to 41 THz *Appl. Phys. Lett.* **76** 3191–3

[34] Brida D, Manzoni C, Cirmi G, Marangoni M, Bonora S, Villoresi P, De Silvestri S and Cerullo G 2010 Few-optical-cycle pulses tunable from the visible to the mid-infrared by optical parametric amplifiers *J. Opt.* **12** 13001

[35] Driscoll T J, Gale G M and Hache F 1994 Ti:sapphire second-harmonic-pumped visible range femtosecond optical parametric oscillator *Opt. Commun.* **110** 638–44

[36] Brida D, Marangoni M, Manzoni C, De Silvestri S and Cerullo G 2008 Two-optical-cycle pulses in the mid-infrared from an optical parametric amplifier *Opt. Lett.* **33** 2901

[37] Alfano R R and Shapiro S L 1970 Emission in the region 4000 to 7000 Å via four-photon coupling in glass *Phys. Rev. Lett.* **24** 584–7

[38] Alfano R R and Shapiro S L 1970 Observation of self-phase modulation and small-scale filaments in crystals and glasses *Phys. Rev. Lett.* **24** 592–4

[39] Reed M K, Steiner-Shepard M K and Negus D K 1994 Widely tunable femtosecond optical parametric amplifier at 250 kHz with a Ti:sapphire regenerative amplifier *Opt. Lett.* **19** 1855

[40] Reed M K, Steiner-Shepard M K, Armas M S and Negus D K 1995 Microjoule-energy ultrafast optical parametric amplifiers *J. Opt. Soc. Am.* B **12** 2229

[41] Reed M K, Armas M S, Steiner-Shepard M K and Negus D K 1995 30 fs pulses tunable across the visible with a 100 kHz Ti:sapphire regenerative amplifier *Opt. Lett.* **20** 605

[42] Bradler M, Baum P and Riedle E 2009 Femtosecond continuum generation in bulk laser host materials with sub-μJ pump pulses *Appl. Phys.* B **97** 561–74

[43] Polli D, Brida D, Mukamel S, Lanzani G and Cerullo G 2010 Effective temporal resolution in pump-probe spectroscopy with strongly chirped pulses *Phys. Rev.* A **82** 1–8

[44] Kane D J and Trebino R 1993 Characterization of arbitrary femtosecond pulses using frequency-resolved optical gating *IEEE J. Quantum Electron.* **29** 571–9

[45] Petrov V, Noack F and Stolzenberger R 1997 Seeded femtosecond optical parametric amplification in the mid-infrared spectral region above 3 μm *Appl. Opt.* **36** 1164

[46] Pashkin A, Junginger F, Mayer B, Schmidt C, Schubert O, Brida D, Huber R and Leitenstorfer A 2013 Quantum physics with ultrabroadband and intense terahertz pulses *IEEE J. Sel. Top. Quantum Electron.* **19** 8401608

[47] Vodopyanov K L and Kulevskii L A 1995 New dispersion relationships for GaSe in the 0.65–18 μm spectral region *Opt. Commun.* **118** 375–8

[48] Sell A, Leitenstorfer A and Huber R 2008 Phase-locked generation and field-resolved detection of widely tunable terahertz pulses with amplitudes exceeding 100 MV/cm *Opt. Lett.* **33** 2767–9

[49] Fischer M P, Bühler J, Fitzky G, Kurihara T, Eggert S, Leitenstorfer A and Brida D 2017 Coherent field transients below 15 THz from phase-matched difference frequency generation in 4H-SiC *Opt. Lett.* **42** 2687

[50] Brabec C J, Gowrisanker S, Halls J J M, Laird D, Jia S and Williams S P 2010 Polymer-fullerene bulk-heterojunction solar cells *Adv. Mater.* **22** 3839–56

[51] Louarn G, Trznadel M, Buisson J P, Laska J, Pron A, Lapkowski M and Lefrant S 1996 Raman spectroscopic studies of regioregular poly(3-alkylthiophenes) *J. Phys. Chem.* **100** 12532–9